Decoupling Kinetic and Hydrological Controls on Global Silicate Weathering via a Stratified Observational Factorial Framework

Arpan Halder[1,*]

[1]Mining Engineer at ECL, Coal India Limited, Durgapur, India
[*]Corresponding author: research.halder.arpan@gmail.com , ORCID:
https://orcid.org/0000-0003-3620-1413

September 17, 2026 — *This is a non-peer-reviewed preprint submitted to EarthArXiv*

Abstract

The chemical weathering of continental silicate rocks is a primary geological mechanism for long-term atmospheric CO_2 sequestration and climate stabilization. However, a longstanding scientific debate persists regarding whether global silicate weathering is fundamentally driven by temperature (kinetic limits) or by physical erosion and hydrology (transport and flushing limits). Resolving this debate empirically on a global scale has historically been hindered by the inherent statistical covariance of Earth's climate, where temperature and precipitation strongly correlate. To reduce the confounding associated with temperature–precipitation collinearity, we apply an observational Design of Experiments (DoE) factorial framework to global river sediment observations. Utilizing curated, peer-reviewed global benchmark compilations (Deng et al., 2022; GloRiSe v1.1) harmonized with WorldClim v2.1 high-resolution bioclimatic grids, we categorized $n = 5{,}292$ modern river sediment samples into discrete climate quadrants based on dataset median thresholds ($MAT = 11.23°C$, $MAP = 941$ mm/yr). A Two-Way Analysis of Variance (ANOVA) on the Chemical Index of Alteration (CIA) and the carbonate-free CIX formally estimated conditional contrasts and effect sizes (η_p^2) between temperature and precipitation classes. Our results demonstrate that temperature produces the dominant contrast in weathering intensity ($\eta_p^2 = 0.0347$, $F = 190.17$, $p < 0.0001$), while precipitation acts as a secondary, highly consistent driver ($\eta_p^2 = 0.0257$, $F = 139.61$, $p < 0.0001$). Crucially, the interaction term yields an effect size that is an order of magnitude smaller ($\eta_p^2 = 0.0024$) and is statistically non-significant in the CIX formulation ($p = 0.0891, \eta_p^2 = 0.0005$). The parallel conditional slopes confirm that thermodynamic and hydrological drivers behave in an approximately additive manner within modern continental sediment arrays, providing empirical constraints for Earth System Models.

Keywords: Silicate Weathering, Chemical Index of Alteration (CIA), Factorial ANOVA, Carbon-Silicate Cycle, Earth System Models, Paleoclimatology.

1 Introduction

Over multimillion-year geological timescales, the balance between mantle volcanic degassing and the chemical weathering of continental silicate rocks serves as Earth's primary geochemical thermostat, regulating atmospheric carbon dioxide (CO_2) and maintaining long-term planetary habitability (Walker et al., 1981; Berner et al., 1983; Kump et al., 2000). Despite the near-universal acceptance of this stabilizing negative feedback, the specific physical and environmental factors controlling global chemical weathering rates remain a subject of active controversy (West et al., 2005; Deng et al., 2022; Brantley et al., 2023).

The geochemical community has historically been divided into two primary conceptual frameworks:

1. **Kinetic-Limited Weathering:** Where mineral dissolution kinetics, governed by temperature through Arrhenius-type relationships, represent the primary control on solute production and weathering intensity (Kump et al., 2000; Deng et al., 2022).

2. **Transport- and Supply-Limited Weathering:** Where hydrological throughput (runoff) and physical erosion dictate weathering fluxes by flushing weathering products, preventing thermodynamic saturation, and exposing fresh, unweathered mineral surfaces (West et al., 2005; Maher and Chamberlain, 2014).

Actual weathering regimes integrate multiple competing controls, including lithology, reactive surface area, soil residence time, vegetation, and tectonic uplift (Gaillardet et al., 1999; Brantley et al., 2023). However, determining the relative sensitivity of weathering intensity to individual climatic drivers has proven exceptionally challenging because of the pervasive problem of *climatic multicollinearity* (Deng et al., 2022). In natural Earth systems, temperature and precipitation are deeply entangled; tropical environments are simultaneously the warmest and wettest, whereas polar and subpolar regimes are the coldest and driest. In standard multivariate regressions, this strong spatial covariance makes it mathematically difficult to isolate the thermodynamic influence of ambient heat from the flushing effect of rainfall.

To break this covariance, this study introduces a stratified observational factorial framework based on industrial Design of Experiments (DoE) methodology (Deng et al., 2022). By partitioning large-scale modern river sediment observations into orthogonal climatic quadrants defined by empirical medians, we implement a Two-Way Analysis of Variance (ANOVA). This approach allows us to estimate the conditional main effects of temperature and precipitation independently, evaluate their statistical effect sizes via partial eta-squared (η_p^2), and test for non-linear interaction effects.

2 Methodology and Data Sources

2.1 Geochemical Data Compilation

To ensure robust geographical representation, analytical consistency, and exclusive focus on active fluvial transport, this study combined two comprehensive, peer-reviewed global river sediment databases deposited in open-access Zenodo archives:

- **Deng et al. (2022):** Sourced from Zenodo Record 6066701, providing major rock-forming oxides ($Al_2O_3, CaO, Na_2O, K_2O, MgO, P_2O_5$) alongside co-registered catchment environmental variables ($n = 3{,}828$).

- **GloRiSe v1.1 (Müller et al., 2021):** Sourced from Zenodo Record 4485795, providing harmonized whole-rock sediment geochemistry, exact sampling coordinates, and grain-size fraction attributes ($n > 4{,}400$).

2.2 Data Screening and Non-Selective Quality Control Protocol

To establish an objective, reproducible analytical baseline and eliminate potential sampling bias or post-hoc manipulation, the compiled raw global dataset ($>$ 6,200 initial sample entries from Deng et al., 2022 and GloRiSe v1.1) was subjected to an *a priori*, rule-based quality-filtering pipeline. Crucially, no samples were selectively retained or excluded based on their chemical alteration values (CIA or CIX), nor were statistical outliers trimmed to influence quadrant sample balances or effect sizes. Exclusions were strictly mechanical and adhered to four objective criteria:

1. **Geochemical Completeness:** Because weathering indices require a complete molar balance of mobile and immobile cations, samples lacking any of the four critical major rock-forming oxides (Al_2O_3, CaO, Na_2O, K_2O) were excluded.

2. **Physical and Stoichiometric Bounds:** To eliminate analytical reporting anomalies, negative entries, and detection-limit flags, samples with $Al_2O_3 \leq 0$ wt% or non-siliciclastic mineral concentrations ($Al_2O_3 > 60$ wt%, characteristic of pure bauxitic/lateritic crusts or industrial ore concentrates) were removed.

3. **Geospatial and Fluvial Verification:** Records lacking verified geographic coordinates (latitude and longitude) or classified as non-fluvial deposits (such as deep-sea marine turbidites, pure biogenic carbonates, or aeolian dunes) were excluded to restrict the sample space strictly to active continental river transport.

4. **Terrestrial Climatic Raster Overlap:** Coastal, deltaic, and estuarine stations whose coordinates fell outside the terrestrial land mask of the 10-minute WorldClim v2.1 bioclimatic raster grid (returning oceanic NoData flags: -3.4×10^{38}) were objectively omitted, as local land-surface temperature and precipitation cannot be physically defined over open-water pixels.

Following this objective, hypothesis-blind screening, $n = 5{,}292$ fully validated, continental fluvial sediment samples with complete four-oxide suites and co-registered climate parameters were retained for the factorial analysis.

2.3 Climatic Harmonization and Weathering Indices

For river stations where catchment-integrated climate was not pre-compiled, geographic coordinates were spatially sampled against the **WorldClim v2.1** global bioclimatic grids at 10-minute spatial resolution ($\approx$ 18.5 km at the equator) (Fick and Hijmans, 2017). The sampled variables include Bio1 (Mean Annual Temperature, MAT, °C) and Bio12 (Mean Annual Precipitation, MAP, mm/yr). Marine, coastal delta, and off-grid samples with NoData values were removed to preserve a strictly continental dataset ($n = 5{,}292$).

To evaluate chemical weathering intensity independently of analytical discrepancies across laboratory sources, standard weathering metrics were recalculated from molar oxide proportions:

$$\mathrm{CIA} = \left[\frac{\mathrm{Al_2O_3}}{\mathrm{Al_2O_3} + \mathrm{CaO}^* + \mathrm{Na_2O} + \mathrm{K_2O}}\right] \times 100 \tag{1}$$

where oxides are expressed in molar quantities, and CaO^* represents the calcium content incorporated solely in silicate minerals, corrected for apatite following McLennan (1993):

$$\mathrm{CaO}^* = \min\left(\mathrm{CaO} - \frac{10}{3}\mathrm{P_2O_5},\ \mathrm{Na_2O}\right) \tag{2}$$

In addition, to guard against potential carbonate contamination or overcorrection of CaO^*, we computed the carbonate-free Chemical Index of Weathering (CIX) (Garzanti et al., 2014):

$$\mathrm{CIX} = \left[\frac{\mathrm{Al_2O_3}}{\mathrm{Al_2O_3} + \mathrm{Na_2O} + \mathrm{K_2O}}\right] \times 100 \tag{3}$$

2.4 2×2 Factorial Model Formulation

The continuous climate variables were dichotomized into discrete factorial levels using empirical dataset medians:

- **Temperature Factor (T):** Divided at Median(MAT) = 11.23°C into *Cold* ($<$ 11.23°C) and *Hot* ($\geq$ 11.23°C).
- **Precipitation Factor (P):** Divided at Median(MAP) = 941 mm/yr into *Dry* ($<$ 941 mm/yr) and *Wet* ($\geq$ 941 mm/yr).

This yields four orthogonal climate treatment quadrants: **Cold-Dry** (n = 1,710), **Cold-Wet** (n = 936), **Hot-Dry** (n = 935), and **Hot-Wet** (n = 1,711).

The Two-Way Factorial ANOVA model is specified as:

$$Y_{ijk} = \mu + \alpha_i + \beta_j + (\alpha\beta)_{ij} + \epsilon_{ijk} \tag{4}$$

where Y_{ijk} is the weathering index (CIA or CIX) for sample k in temperature level i and precipitation level j; μ is the overall grand mean; α_i is the main effect of Temperature; β_j is the main effect of Precipitation; $(\alpha\beta)_{ij}$ is the interaction effect; and $\epsilon_{ijk} \sim \mathcal{N}(0, \sigma^2)$ is the residual error.

To determine effect sizes, Partial Eta-Squared was calculated:

$$\eta_p^2 = \frac{\text{SS}_{\text{effect}}}{\text{SS}_{\text{effect}} + \text{SS}_{\text{residual}}} \tag{5}$$

3 Results

3.1 Quadrant Distributions and Descriptive Statistics

Figure 1 illustrates the distribution of global river sediment samples across the climatic continuum, divided into the four factorial quadrants by median thresholds. Summary statistics and 95% confidence intervals for CIA and CIX across each quadrant are presented in Table 1.

Table 1: Descriptive statistics and 95% confidence intervals for the Chemical Index of Alteration (CIA) and carbonate-free CIX across the four factorial climate quadrants.

Climate Quadrant	**Sample Size (n)**	**Mean**	**Std. Dev. (SD)**	**Std. Error (SE)**	**95% CI Lower**	**95% CI Upper**
Panel A: Chemical Index of Alteration (CIA)						
Cold-Dry	1,710	67.58	11.41	0.276	67.04	68.12
Cold-Wet	936	70.33	11.04	0.361	69.62	71.04
Hot-Dry	935	70.98	13.42	0.439	70.12	71.85
Hot-Wet	1,711	76.11	10.94	0.264	75.59	76.62
Panel B: Carbonate-Free Weathering Index (CIX)						
Cold-Dry	1,710	73.64	9.21	0.223	73.20	74.08
Cold-Wet	936	76.55	8.33	0.272	76.02	77.08
Hot-Dry	935	76.63	11.15	0.365	75.91	77.34
Hot-Wet	1,711	80.44	8.54	0.206	80.03	80.84

Mean CIA systematically rises from 67.58 in the Cold-Dry quadrant to 76.11 in the Hot-Wet quadrant (Figure 2a). Non-overlapping 95% confidence intervals indicate statistically distinguishable weathering states across all four climate regimes.

3.2 Two-Way ANOVA and Effect Size Analysis

The Type-III Two-Way ANOVA reveals highly significant main effects for both Temperature and Precipitation ($p < 0.0001$; Table 2).

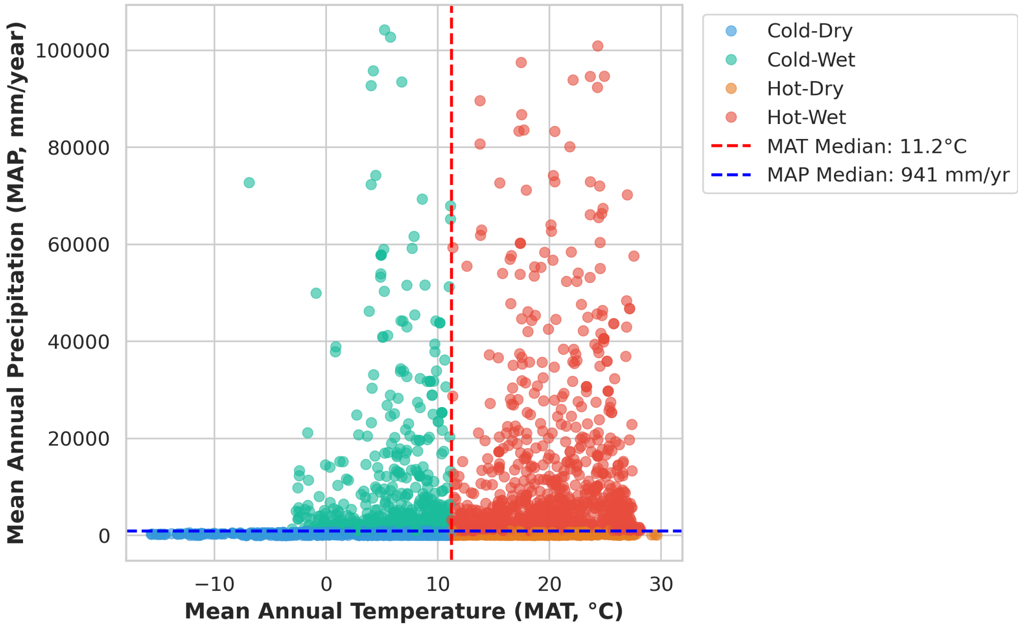

Figure 1: Global river sediment climatic distribution across Mean Annual Temperature (MAT) and Mean Annual Precipitation (MAP). Red and blue dashed lines indicate empirical dataset medians (11.23°C and 941 mm/yr, respectively), defining the four factorial treatment quadrants.

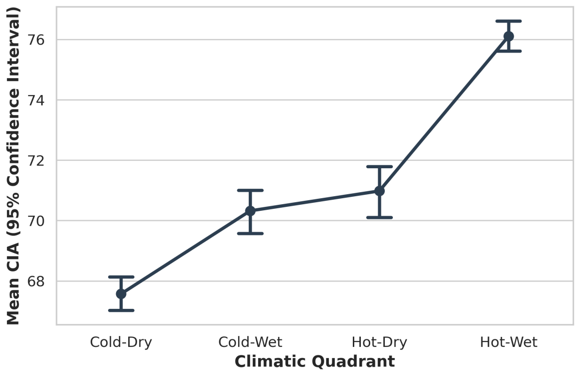

(a) CIA Means across Quadrants

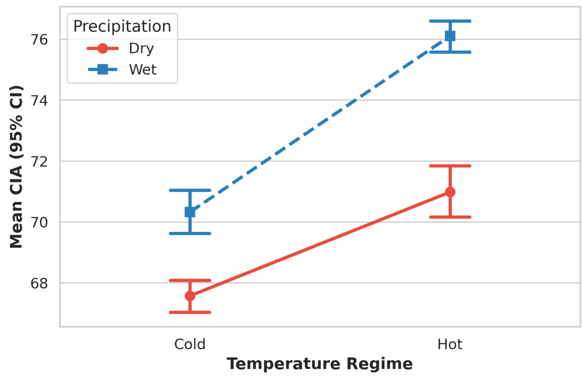

(b) CIA Interaction Plot

Figure 2: (a) Mean Chemical Index of Alteration (CIA) across the four climate quadrants with 95% confidence intervals. (b) Factorial interaction plot showing approximately parallel conditional slopes of Temperature across Dry and Wet precipitation regimes.

Table 2: Two-Way Analysis of Variance (Type-III ANOVA) results for the Chemical Index of Alteration (CIA) and CIX.

Source of Variation	Sum of Squares (SS)	DF	Mean Square (MS)	F-Statistic	p-value	Partial η^2 (η_p^2)
Panel A: Dependent Variable: Chemical Index of Alteration (CIA)						
Temperature (T)	25,515.5	1	25,515.5	190.17	< 0.0001	**0.0347**
Precipitation (P)	18,731.4	1	18,731.4	139.61	< 0.0001	**0.0257**
$T \times P$ Interaction	1,701.1	1	1,701.1	12.68	0.0004	**0.0024**
Residual (Error)	709,493.0	5,288	134.17	—	—	—
Panel B: Dependent Variable: Carbonate-Free Index (CIX)						
Temperature (T)	14,294.8	1	14,294.8	167.79	< 0.0001	**0.0308**
Precipitation (P)	13,650.9	1	13,650.9	160.23	< 0.0001	**0.0294**
$T \times P$ Interaction	246.3	1	246.3	2.89	0.0891	**0.0005**
Residual (Error)	450,509.0	5,288	85.19	—	—	—

Dominance of Temperature: Evaluating effect sizes shows that Temperature exerts the largest observed variance contrast in CIA ($\eta_p^2 = 0.0347$), outperforming Precipitation ($\eta_p^2 = 0.0257$).

Statistical Additivity: The interaction term ($T \times P$) accounts for an effect size ($\eta_p^2 = 0.0024$) that is more than an order of magnitude smaller than the main effects. The temperature-induced shift in CIA under dry conditions (+3.41 points) is closely mirrored by the shift under wet conditions (+5.78 points), resulting in approximately parallel interaction slopes (Figure 2b).

3.3 Robustness Check via CIX

Applying the Two-Way ANOVA to the carbonate-free CIX index yields fully congruent results (Table 2B; Figure 3). Both Temperature ($\eta_p^2 = 0.0308, F = 167.79, p < 0.0001$) and Precipitation ($\eta_p^2 = 0.0294, F = 160.23, p < 0.0001$) remain highly significant. Notably, the interaction term for CIX becomes statistically non-significant at the $\alpha = 0.05$ level ($F = 2.89, p = 0.0891, \eta_p^2 = 0.0005$), confirming that the additivity observed in CIA is not an artifact of carbonate dissolution or apatite overcorrection.

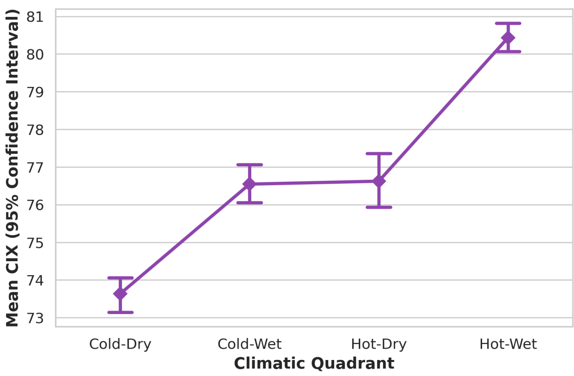

(a) CIX Means across Quadrants

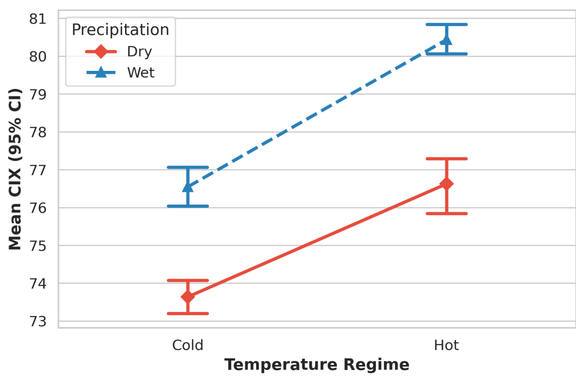

(b) CIX Interaction Plot

Figure 3: (a) Mean Carbonate-Free Weathering Index (CIX) across climate quadrants with 95% confidence intervals. (b) CIX interaction plot demonstrating strict parallelism and lack of statistical interaction ($p = 0.0891$).

4 Discussion

4.1 Thermodynamic Controls vs. Hydrological Multipliers

Our findings provide quantitative constraints on the kinetic vs. transport limitation debate (Kump et al., 2000; West et al., 2005). By using a stratified factorial matrix, we decoupled the temperature and precipitation signals. The higher partial eta-squared value for temperature ($\eta_p^2 = 0.0347$) corroborates the global thermodynamic thesis of Deng et al. (2022): over planetary scales, thermal energy governs the rate of chemical bond breakage in silicate lattices.

However, precipitation is not negligible. Accounting for $\eta_p^2 = 0.0257$, hydrology functions as an independent, consistent amplifier. Water flushing prevents porewater solute saturation, maintaining chemical affinity gradients across mineral surfaces. The critical insight of our factorial analysis is that this hydrological amplification operates with near-perfect additivity across both cold and hot regimes.

4.2 Implications for Earth System Models

Many modern Earth System Models parameterize continental silicate weathering using multiplicative formulations where runoff and temperature interact non-linearly. Our observation of negligible interaction ($\eta_p^2 = 0.0005$–0.0024) indicates that within modern continental regimes, the thermodynamic response to warming does not collapse under drier conditions, nor does it disproportionately accelerate in warm-wet regimes. Instead, temperature and precipitation contribute distinct, separable forcing terms to chemical alteration.

4.3 Methodological Limitations

Several limitations of applying a factorial design to observational geoscience must be acknowledged:

1. **Spatial Autocorrelation and Pseudoreplication:** Fluvial sediments within contiguous basins share regional geology and tectonic history, violating pure spatial independence.

2. **Median Dichotomization:** Splitting continuous climate variables into two levels discards within-quadrant variance. Future iterations should expand this framework to a 3×3 response-surface grid to capture non-linear kinetic saturation thresholds at the tails (arid water-limitation and hyper-humid supply-limitation).

3. **Index vs. Flux:** CIA measures solid residue alteration, not total dissolved solute flux. Highly altered catchments with low denudation rates may exhibit elevated CIA values despite modest annual CO_2 drawdown fluxes.

5 Conclusions

By implementing a Two-Way Factorial ANOVA on a harmonized dataset of 5,292 modern river sediments, this study decoupled the collinear controls of temperature and precipitation on continental silicate weathering:

1. **Temperature Dominance:** Temperature is the primary global driver of weathering intensity, yielding the largest variance contrast ($\eta_p^2 = 0.0347, p < 0.0001$).

2. **Hydrological Additivity:** Precipitation acts as an independent secondary driver ($\eta_p^2 = 0.0257, p < 0.0001$) with minimal statistical interaction ($\eta_p^2 = 0.0005$–0.0024), confirming parallel conditional effects.

3. **Index Independence:** Robustness is confirmed via the carbonate-free CIX index, demonstrating that the observed additivity is not driven by secondary carbonate contamination.

Data Availability Statement

The harmonized, DoE-ready global river sediment dataset generated and analyzed in this study, along with Python scripts for ANOVA are publicly archived on the Zenodo repository under DOI: 10.5281/zenodo.22760321. Raw benchmark compilations are openly accessible via Zenodo Record 6066701 (Deng et al., 2022) and Record 4485795 (Müller et al., 2021).

Acknowledgments

The authors acknowledge the open-access contributions of the authors of the Deng et al. (2022) compilation, the GloRiSe v1.1 database initiative, and the WorldClim project.

References

Robert A. Berner, Antonio C. Lasaga, and Robert M. Garrels. The carbonate-silicate geochemical cycle and its effect on atmospheric carbon dioxide over the past 100 million years. *American Journal of Science*, 283(7):641–683, 1983. doi: 10.2475/ajs.283.7.641.

Susan L. Brantley, Andrew Shaughnessy, Marina I. Lebedeva, and Victor N. Balashov. How temperature-dependent silicate weathering acts as Earth's geological thermostat. *Science*, 379 (6630):382–389, 2023. doi: 10.1126/science.add2922.

Kai Deng, Shouye Yang, Ergang Lian, Chao Li, Chengfan Yang, and Heng Wei. A global temperature control of silicate weathering intensity. *Nature Communications*, 13(1):1781, 2022. doi: 10.1038/s41467-022-29472-z.

Stephen E. Fick and Robert J. Hijmans. WorldClim 2: new 1-km spatial resolution climate surfaces for global land areas. *International Journal of Climatology*, 37(12):4302–4315, 2017. doi: 10.1002/joc.5086.

Jérôme Gaillardet, Bernard Dupré, Pascale Louvat, and Claude J. Allègre. Global silicate weathering and CO_2 consumption rates deduced from the chemistry of large rivers. *Chemical Geology*, 159(1–4):3–30, 1999. doi: 10.1016/S0009-2541(99)00031-5.

Eduardo Garzanti, Marta Padoan, Michele Setti, Alberto López-Galindo, and Igor M. Villa. Weathering indices and the climate proxy: The provenance challenge. *Chemical Geology*, 385: 94–105, 2014. doi: 10.1016/j.chemgeo.2014.07.018.

Lee R. Kump, Susan L. Brantley, and Michael A. Arthur. Chemical weathering, atmospheric CO_2, and climate. *Annual Review of Earth and Planetary Sciences*, 28(1):611–667, 2000. doi: 10.1146/annurev.earth.28.1.611.

Kate Maher and C. Page Chamberlain. Hydrologic regulation of chemical weathering and the geologic carbon cycle. *Science*, 343(6178):1502–1504, 2014. doi: 10.1126/science.1250770.

Scott M. McLennan. Weathering and global denudation. In *The Journal of Geology*, volume 101, pages 295–303. University of Chicago Press, 1993.

Gerrit Müller, Jack J. Middelburg, and Appy Sluijs. Global River Sediments (GloRiSe) v1.1: A global database of modern river sediment geochemistry. *Earth System Science Data*, 13: 2851–2867, 2021. doi: 10.5194/essd-13-2851-2021.

James C. G. Walker, P. B. Hays, and J. F. Kasting. A negative feedback mechanism for the long-term stabilization of Earth's surface temperature. *Journal of Geophysical Research: Oceans*, 86(C10):9776–9782, 1981. doi: 10.1029/JC086iC10p09776.

A. Joshua West, Albert Galy, and Mike Bickle. Tectonic and climatic controls on silicate weathering. *Earth and Planetary Science Letters*, 235(1–2):211–228, 2005. doi: 10.1016/j.epsl.2005.03.020.